ENVIRONMENTAL RESEARCH
LETTERS

LETTER · OPEN ACCESS

Using structure to model function: incorporating canopy structure improves estimates of ecosystem carbon flux in arctic dry heath tundra

To cite this article: Elizabeth Min *et al* 2023 *Environ. Res. Lett.* **18** 065004

ENVIRONMENTAL RESEARCH
LETTERS

OPEN ACCESS

RECEIVED
17 January 2023

REVISED
24 March 2023

ACCEPTED FOR PUBLICATION
20 April 2023

PUBLISHED
12 May 2023

LETTER

Using structure to model function: incorporating canopy structure improves estimates of ecosystem carbon flux in arctic dry heath tundra

Elizabeth Min[1], Shahid Naeem[2], Laura Gough[3], Jennie R McLaren[4], Rebecca J Rowe[5], Edward Rastetter[6], Natalie Boelman[7] and Kevin L Griffin[1,2,7,*]

[1] Department of Earth and Environmental Science, Columbia University, New York, NY, United States of America
[2] Department of Ecology, Evolution, and Environmental Biology, Columbia University, New York, NY, United States of America
[3] Department of Biological Sciences, Towson University, Towson, MD, United States of America
[4] Department of Biological Sciences, The University of Texas at El Paso, El Paso, TX, United States of America
[5] Department of Natural Resources and the Environment, University of New Hampshire, Durham, NH, United States of America
[6] The Ecosystems Center, Marine Biological Laboratory, Woods Hole, MA, United States of America
[7] Lamont-Doherty Earth Observatory, Columbia University, Palisades, NY, United States of America
[*] Author to whom any correspondence should be addressed.

E-mail: griff@LDEO.columbia.edu

Keywords: net ecosystem exchange, low arctic, herbivory, tundra vegetation, ecosystem respiration, gross primary production, structure-from-motion

Supplementary material for this article is available online

Abstract

Most tundra carbon flux modeling relies on leaf area index (LAI), generally estimated from measurements of canopy greenness using the normalized difference vegetation index (NDVI), to estimate the direction and magnitude of fluxes. However, due to the relative sparseness and low stature of tundra canopies, such models do not explicitly consider the influence of variation in tundra canopy structure on carbon flux estimates. Structure from motion (SFM), a photogrammetric method for deriving three-dimensional (3D) structure from digital imagery, is a non-destructive method for estimating both fine-scale canopy structure and LAI. To understand how variation in 3D canopy structure affects ecosystem carbon fluxes in Arctic tundra, we adapted an existing NDVI-based tundra carbon flux model to include variation in SFM-derived canopy structure and its interaction with incoming sunlight to cast shadows on canopies. Our study system consisted of replicate plots of dry heath tundra that had been subjected to three herbivore exclosure treatments (an exclosure-free control [CT], large mammals exclosure), and a large and small mammal exclosure [ExLS]), providing the range of 3D canopy structures employed in our study. We found that foliage within the more structurally complex surface of CT canopies received significantly less light over the course of the day than canopies within both exclosure treatments. This was especially during morning and evening hours, and was reflected in modeled rates of net ecosystem exchange (NEE) and gross primary productivity (GPP). We found that in the ExLS treatment, SFM-derived estimates of GPP were significantly lower and NEE significantly higher than those based on LAI alone. Our results demonstrate that the structure of even simple tundra vegetation canopies can have significant impacts on tundra carbon fluxes and thus need to be accounted for.

1. Introduction

Variation in canopy structure can significantly influence the light environment experienced by leaves within the canopy (Monsi *et al* 2005) and consequently photosynthetic activity (Brunner 1998). As such, canopy structure can play a major role in controlling the net exchange of carbon between an ecosystem and the atmosphere (i.e. net ecosystem exchange (NEE)), and thus in determining ecosystem C sink strength (Kramer *et al* 2002). Due to the relatively low stature of Arctic tundra, it may be tempting to assume that canopy structure plays an insignificant role in controlling tundra carbon fluxes, yet this

assumption is rarely tested (n.b. Williams *et al* 2014). To date, carbon dioxide (CO_2) flux chamber studies (Virkkala *et al* 2018), larger scale eddy flux studies (Rastetter *et al* 2010, Stoy *et al* 2013) and regional scale aircraft and satellite studies (Stow *et al* 1998, Zulueta *et al* 2011) have typically relied on estimations of leaf area index (LAI) derived from normalized difference vegetation index (NDVI) (Street *et al* 2007) to incorporate how variation in vegetation canopies influence NEE. Similarly, current tundra carbon exchange models use LAI (in conjunction with air temperature and light) to predict NEE (Shaver *et al* 2007). However, recent evidence of significant photosynthetic partitioning within low statured tundra canopies (Magney *et al* 2016) suggests that shadows cast within tundra canopies have a significant impact on the amount of light reaching foliage. As such, canopy structure will need to be taken into account in tundra carbon models as overreliance on LAI alone likely introduces error in estimates of canopy photosynthetic rates and net carbon flux (Sprintsin *et al* 2012). Lending further motivation to explicitly account for tundra canopy structure, the low sun angles that typify arctic ecosystems cause dramatic, diurnal dynamics in shadow patterns and light quality that interact with spatial variation in tundra canopy structure to have an outsized impact on light available within tundra canopies for photosynthesis (Stow *et al* 2004, Buchhorn *et al* 2016).

While NDVI has been shown to identify small spatial differences in maximum woody shrub height before peak leaf out, once leaves are fully expanded during peak growing season, NDVI and thus LAI more closely tracks variation in canopy cover rather than structure (Boelman *et al* 2011). Traditional methods for quantifying canopy structure are time consuming, prone to substantial error, and have relatively low spatial resolution (Wall *et al* 1991, Bréda 2003, Weiss *et al* 2004). Fortunately, recent advances in remote sensing have enabled rapid, fine-scale, and three-dimensional (3D) quantification of canopy structure (Zellweger *et al* 2019). For example, many studies make use of light detection and ranging (LiDAR) technology to quantify the structure of plant canopies, including tundra canopies, from either spaceborne, airborne and terrestrial sensors (Omasa *et al* 2007, Greaves *et al* 2015, Friedli *et al* 2016, Magney *et al* 2016). In addition, structure from motion (SFM) techniques that use two-dimensional photographs captured in sequence from a suite of view angles, are being increasingly used as an alternative to LiDAR (Ighaut *et al* 2019). Using SFM specific software, the photographs are converted to point cloud reconstructions of fine-scale plant canopy structure products similar to those generated using LiDAR (Mathews and Jensen 2013, Zellweger *et al* 2019, Alonzo *et al* 2020, Mesas-Carrascosa *et al* 2020). Importantly however, a major advantage of using SFM over LiDAR technology is that consumer grade RGB cameras can be used instead of specialized LiDAR instruments (Westoby *et al* 2012, Cunliffe *et al* 2016, Shafian *et al* 2018), making SFM a more affordable and widely accessible means of assessing vegetation structure and height. In addition, this method produces a point cloud with color information per point that allows for color based classification methods. Although SFM has been used to map tall shrub biomass in arctic tundra ecosystems (Alonzo *et al* 2020, Cunliffe *et al* 2020), it is a relatively new technique that has yet to be widely adopted.

Our overall goal is to understand how variation in 3D canopy structure interacts with diurnal dynamics in sun angle to determine ecosystem carbon uptake in arctic tundra during the period of peak leaf out. To achieve this goal, our objective was to use a SFM-based approach, combined with color vegetation indices and hourly data on ambient light levels and sun angle, to estimate the amount of carbon fixed over the course of a single day by dry heath tundra canopies that differ in 3D structure. We hypothesized that periods of substantial surface canopy shading occur, primarily in more structurally complex canopies and during early morning and late evening hours when both the sun altitude and ambient light levels are low. In turn, this may result in lower estimated rates of CO_2 uptake than those previously estimated by Min *et al* (2021) for the same dry heath canopies.

2. Methods

2.1. Study site and approach

2.1.1. Study site

Our study was conducted at the Arctic long term ecological research (LTER) site at Toolik Lake in northern Alaska (68.2 °N, 149.6 °W, 760 m a.s.l.) where a long-term study of mammalian herbivory provided for a range of canopy structures. Briefly, a long-term herbivory experiment was established in 1996 in a dry heath tundra community, which is largely composed of lichen and dwarf deciduous and evergreen shrubs. The experimental design consists of three replicate blocks of 5 m × 20 m plots. Each block had one plot with a 5 m × 10 m exclosure-free portion [CT] that was accessible to herbivores, and a 5 m × 10 m fenced portion surrounded by a large-mesh (15.2 cm × 15.2 cm mesh) fence to exclude only large herbivores such as caribou (*Rangifer tarandus*). This fenced area was divided in half, with one 5 × 5 m half further surround by a small-mesh fence (1.3 cm × 1.3 cm mesh) to additionally exclude small mammals, such as singing voles (*Microtus miurus*). This resulted in two different herbivore exclosure treatments per block, with one excluding only large herbivores [ExL], and the other excluding both large and small herbivores [ExLS] (Gough *et al* 2007). The experimental set up and local environmental conditions are fully described elsewhere (Min *et al* 2021 and references there in). In each

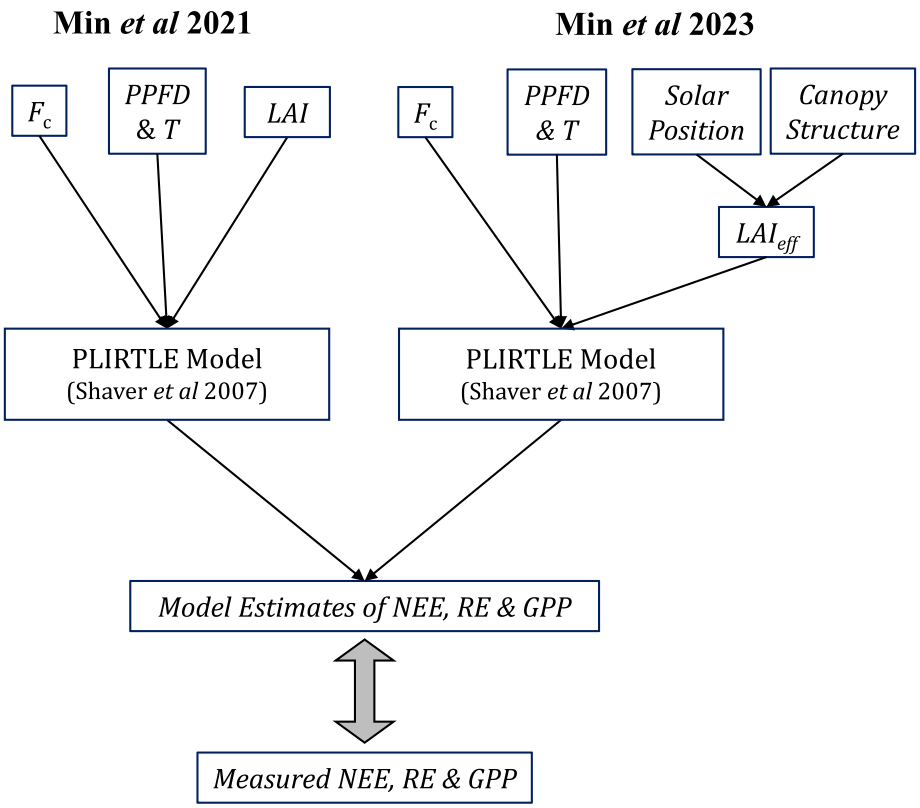

Figure 1. Logic flow for analyzing Net Ecosystem Exchange (NEE, mmol CO_2 m^{-2} ground s^{-1}) in dry heath tundra community. The standard approach used by Min *et al* (2021) combines carbon flux measurements (Fc ; mmol CO_2 m^{-2} ground s^{-1}) made by Min *et al* (2021), with environmental data (PPFD, photosynthetic proton flux density; mmol photons m^{-2} ground s^{-1}) and T, air temperature; °C) and the Leaf Area Index (LAI, m^2 leaf m^{-2} ground) estimated from measurements of spectral reflectance (i.e. NDVI) to fit the PLIRTLE model of Shaver *et al* (2007) and partition the observed NEE to the component fluxes of photosynthesis and respiration (GPP and RE, both in mmol CO_2 m^{-2} ground s^{-1}). The current approach incorporates canopy structure (using Structure From Motion (SFM)), and solar ray tracing to determine the fully illuminated and green (i.e. photosynthetically effective) leaf area index (LAIeff), thus accounting for shade within the canopy. LAIeff is substituted for LAI when fitting the GPP portion of PLIRTLE. Finally, carbon flux partitioning between GPP and RE from these two modeling approaches can be compared to the measured fluxes (see Min *et al* 2021) to assess strength of the model fits.

treatment plot, the measurements described below were made within three circular subplots (75.5 cm diameter) that were selected arbitrarily but at least 0.5 m away from the fences to avoid significant shading and artifacts due to slight changes in snow accumulation immediately next to the fences. As the fences were constructed of thin posts and wire mesh, we do not expect the fences to cast significant amounts of shadow on the subplots aside from when the sun angle and light is lowest, minimizing their impact on our results. All measurements were made between 14 July and 28 July 2017, when the tundra's leaf out was at its characteristic annual peak (Shaver and Chapin 1991, Johnson *et al* 2000). We stress, this current study is not focused on the *cause* of the observed differences in canopy structure among treatment plots (i.e. herbivory) but instead takes advantage of the *resulting* variation in canopy structure of the plots.

2.1.2. Overview of study approach

We assess the impact of spatial variation in canopy structure (from SFM) on estimates of NEE by comparing them to previous estimates of NEE that were based only on spatial variation in LAI (from NDVI) (Min *et al* 2021). By quantifying 3D canopy structure and using light ray tracing, we consider only the surface area of green (i.e. photosynthetically active) portions of the canopy that were illuminated as the sun progressed through the ecliptic plane during a 24 h period in late July. The flow chart shown in figure 1 summarizes the main steps taken in the SFM-based approach used to accomplish this, and compares it to an NDVI-based approach previously used by Min *et al* (2021) on the same tundra canopies. Details on each of the main steps used in the current approach are described in the sections below.

2.2. SFM: canopy surface roughness and 3D structure

Photographs were taken of each subplot using five consumer grade red, green and blue (RGB) wavelength cameras (HERO5, GoPro, San Mateo, CA, USA). The cameras were mounted on the vertical arc of a custom hemispherical and rotatable rig attached to a circular base with an inner diameter of 75.5 cm (i.e. slightly larger than subplots) (figure 2). The rig and base were centered over each subplot with cameras facing inward. To ensure sufficient overlap between images for subsequent processing, the rig was systematically rotated a total of 360°, with a photograph taken from all five cameras every 3°–5° of rotation (Forlani *et al* 2018). This resulted in hundreds of overlapping photographs per subplot. An external marker was placed directly adjacent to the subplot to indicate north in each photograph.

An image processing software (PhotoScan Professional Edition, Agisoft LLC, St. Petersburg, Russia) was used to convert the combination of photographs taken of each individual subplot into a 3D point cloud. A free 3D point cloud processing software (CloudCompare (version 2.10.2), GPL, retrieved from www.cloudcompare.org/) was used to digitally level, center at the origin, orient north and scale each point cloud, using the camera rig as a reference. In order to exclude areas of each subplot that were in shadow cast by the rig and/or those distorted around the edges of the subplot photograph, a rectangular area representing 26% of the total subplot area was clipped from the center of each point cloud.

A digital surface map (DSM) of the canopy was generated from each subplot's point cloud using the point to raster method as implemented in the 'lidR' package (Roussel *et al* 2020) in R (Team R C 2013). This 3D representation of canopy surface structure is made up of 'voxels' that define each point in three-dimensional space. To estimate canopy surface roughness, subplot level terrain ruggedness index (TRI) was calculated from each DSM, as implemented in the 'raster' package (Hijmans *et al* 2015) in R (Team R C 2013). TRI values range from 0 (smooth surface) to 1 (rough surface).

2.3. Effective LAI (LAI_{eff})

To estimate the average hourly 'effective LAI' (LAI_{eff}, defined as the LAI of only illuminated (i.e. not in shadow), green (i.e. photosynthetically active) vegetation in each subplot), we overlaid the voxels representing the 3D canopy surface structure from the DSM (see section 2.2) with color information from the point cloud to determine whether each voxel was dominated by green vs. non-green points, as well as hourly dynamics in ambient light levels (i.e. photosynthetic photon flux density (PPFD) and solar position (figure 1). The paragraphs below provide details on each of these steps.

The average hourly rate of PPFD (μmol photons m^{-2} ground s^{-1})—hereafter referred to as photosynthetically active radiation (PAR)—was calculated from continuous measurements made on a single cloudless day (28 July 2017) (Toolik Field Station Environmental Data Center). To determine incident sun angles, the NOAA Solar Calculator (US Department of Commerce *et al* 2005) was used to determine solar position for each hour of the day. The average hourly rate of PAR that reached each voxel (PAR_{veg}) was determined using the 'rayshader' package (Morgan-Wall 2020) in R (Team R C 2013) which combined information on ambient PAR, incident sun angle and 3D canopy surface structure. The path of individual rays of PAR were traced through the subplot's DSM, generating 25 hourly shade maps showing shade depth per voxel. Average hourly ambient PAR values were then scaled as a function of average hourly shade depth. This yielded 25 hourly estimates of PAR_{veg} per voxel for each subplot on 28 July 2017. The rayshader model incorporates Lambertian reflectance (Morgan-Wall 2020) and assumes a diffusely reflecting matte surface (Koppal 2014), providing an approximation of reflection for the canopy (Verhoef 1984). Light transmission through the leaf is not taken into account but typically less than 5% of radiation in the photosynthetically active range is transmitted (Massa *et al* 2015) and is thus unlikely to significantly influence our conclusions. Future modeling efforts could test this assumption directly.

In order to distinguish between voxels dominated by green or non-green vegetation in each subplot, we used color vegetation indices (CVI). Prior to calculating CVI values, RGB reflectance values (*r, g* and *b*) from the point clouds (see section 2.2) were normalized according to equations (1) and (2):

$$r = \frac{R}{R+G+B}\ g = \frac{G}{R+G+B}\ b = \frac{B}{R+G+B} \quad (1)$$

where *R, G* and *B* are normalized values of RGB for each point calculated as:

$$R = \frac{\text{red}}{255}\ G = \frac{\text{green}}{255}\ B = \frac{\text{blue}}{255} \quad (2)$$

and where red, green, and blue are derived from raw image data from the GoPro cameras and 255 is the maximum signal for each of these three bands. A suite of six CVIs that have previously been demonstrated to emphasize the green component of images (the defining trait of green vegetation) were calculated using the *r, g*, and *b* values. The CVIs that were calculated were: excess of blue (Mao *et al* 2003), excess of green (Woebbecke *et al* 1995), excess of red (Meyer *et al* 1999), excess of green minus excess red (Neto 2004), color index of vegetation extraction (Kataoka *et al* 2003) and the normal green-red difference index (Woebbecke *et al* 1993, Mesas-Carrascosa *et al* 2020). To determine which of the six CVIs provides the best discrimination between green and non-green vegetation cells, an *M*-statistic (*M*) was calculated according to equation (3):

Figure 2. Photograph of camera and rig set up. The pin flags and clamp outside the base were used to indicate north. Five GoPro cameras were attached along the inner edge of the vertical arc. Photograph shows a control plot.

$$M = \left(\mu_{\text{vegetation}} - \mu_{\text{non-green vegetation}}\right) / \left(\sigma_{\text{vegetation}} - \sigma_{\text{non-green vegetation}}\right) \quad (3)$$

where μ and σ are the mean and standard deviation of both classes, respectively. Values of M lower than 1 indicate poor class discrimination, while values of M higher than 1 indicate adequate class discrimination. The excess of green was the only CVI with an M-value greater than 1 and thus was the only CVI able to classify voxels as either green vegetation or non-green vegetation. Each subplot was then randomly sampled for 100 000 points and associated excess of green values were calculated. Otsu's method, an algorithm commonly applied to perform automatic image thresholding (Goh *et al* 2018), was used to identify a threshold value of excess of green that separates the two classes. This method was applied 100 times per subplot and the resulting 100 threshold values were averaged to calculate the final threshold value used to classify each voxel as either green or non-green vegetation.

We then used element-wise multiplication of each subplot's green vegetation and average hourly PAR_{veg} matrices to calculate the average hourly PAR levels incident on green vegetation voxels (PAR_{Gveg}) for each subplot. Daily sums of PAR_{Gveg} per subplot were calculated by integrating the 25 average hourly values for each voxel. Finally, LAI_{eff} was calculated by dividing the number of illuminated, green vegetation voxels (in the PAR_{Gveg} matrix) for a given hour, divided by the total number of voxels per subplot. These subplot level LAI_{eff} values were used in the calculation of $GPPLAI_{eff}$ (see equation (9)).

2.4. LAI

Since the process of foliar respiration does not require light, in addition to LAI_{eff}, we calculated LAI per subplot by dividing the number of all green vegetated voxels by the total number of voxels in each subplot. These LAI values were used in the calculation of RE_{LAI} (see equation (8)), as well as in GPP_{LAI} which was compared with GPP LAI_{eff} (see section 2.5).

2.5. Modeled canopy carbon fluxes

The same widely used NEE (μmol CO_2 m^{-2} ground s^{-1}) model (PLIRTLE, Shaver *et al* 2007) (equations (4)–(6)) and model parameters were used

as in our previous study (Min *et al* 2021) to estimate carbon fluxes for each hour of 28 July 2017, in each subplot (figure 1),

$$\mathrm{NEE} = \mathrm{RE} - \mathrm{GPP} \tag{4}$$

$$\mathrm{RE} = (R_0 * \mathrm{LAI} + R_x)\, \mathrm{e}^{\beta * T} \tag{5}$$

$$\mathrm{GPP} = \frac{P_{\mathrm{maxL}} * \mathrm{LAI} * E_0 * \mathrm{PAR}}{P_{\mathrm{maxL}} + E_0 * \mathrm{PAR}} \tag{6}$$

where RE is ecosystem respiration (μmol CO_2 m^{-2} ground s^{-1}), GPP is gross primary productivity (μmol CO_2 m^{-2} ground s^{-1}), each of R_0 (μmol m^{-2} leaf s^{-1}), R_x (μmol m^{-2} ground s^{-1}) and β ($^{\circ}C^{-1}$) are empirically derived respiration parameters, T is air temperature inside the chamber (°C), P_{maxL} is the theoretical light saturated photosynthesis rate (μmol m^{-2} leaf s^{-1}), LAI is canopy LAI (m^2 leaf m^{-2} ground), E_0 is the light use efficiency (μmol CO_2 μmol^{-1} photons), and PAR is the PAR at the top of the canopy (μmol photons m^{-2} ground s^{-1}). R_0, R_x and β values were restricted to values $\geqslant 0$.

However, to take into account shade cast by canopy structure as determined by our SFM-based approach, the following modifications to the LAI and PAR terms used to calculate fluxes were made (equations (7)–(9)). First, to estimate hourly rates of gross primary productivity (GPP $\mathrm{LAI_{eff}}$) we used average hourly $\mathrm{LAI_{eff}}$ and $\mathrm{PAR_{Gveg}}$ values (equation (9)). Second, to estimate hourly rates of ecosystem respiration ($\mathrm{RE_{LAI}}$) we used LAI (equation (8)). Daily flux values were calculated by integrating hourly flux estimates over the entire 24 h period,

$$\mathrm{NEE_{LAIeff}} = \mathrm{RE_{LAI}} - \mathrm{GPP_{LAIeff}} \tag{7}$$

$$\mathrm{RE_{LAI}} = (R_0 * \mathrm{LAI} + R_x)\, \mathrm{e}^{\beta * T} \tag{8}$$

$$\mathrm{GPP_{LAIeff}} = \frac{P_{\mathrm{maxL}} * \mathrm{LAI_{eff}} * E_0 * \mathrm{PAR_{Gveg}}}{P_{\mathrm{maxL}} + E_0 * \mathrm{PAR_{Gveg}}}. \tag{9}$$

2.6. Statistical analysis

Data were analyzed using linear mixed effects models with block as a random effect and either treatment or method as a fixed effect depending on the data being compared. Maximum likelihood estimation was used to obtain p-values for fixed effects. The Kenward–Roger method was used to obtain *p*-values for differences among treatments when applicable. *P*-values less than 0.05 were considered significant. Model residuals were checked for normality. In cases where the residuals were non-normal, data were log transformed before performing statistical tests. In the rare case that the transformed data remained non-normal, outliers, defined as data points beyond 1.5 times the interquartile range, were removed. Unless otherwise noted, statistical analyses were done in R v. 3.5.1 (Team R C 2013), and the following packages were used to calculate statistics: lme4 (Bates *et al* 2015), lmerTest (Kuznetsova *et al* 2017), and lsmeans (Lenth 2016).

3. Results

3.1. Canopy surface roughness

There was a statistically significant difference in the canopy surface roughness, estimated via TRI, between the CT and each of the long-term treatments (figure 3). Relative to CT, the mean TRI for ExL was 37% lower, and ExLS was 22% lower, indicating that the canopy surface of the CT subplots has more variation in canopy heights.

3.2. Light received by green vegetation throughout the day

Over the course of the day, the hourly mean $\mathrm{PAR_{Gveg}}$ of each treatment changed dramatically, ranging from 0 μmol photons m^{-2} s^{-1} at midnight to a maximum of ~1100 μmol photons m^{-2} s^{-1} at 2 pm (i.e. solar noon) (figure 4). Throughout the day there were statistically significant differences in $\mathrm{PAR_{Gveg}}$ between CT and each of the exclosure treatments. Relative to CT, $\mathrm{PAR_{Gveg}}$ for ExL was higher in nearly all hours of the day between 5 am and midnight (except for 9 am and 10 am), while $\mathrm{PAR_{Gveg}}$ for ExLS was higher during only late afternoon through evening hours (i.e. from 4 pm through 10 pm) (figure 5). No statistically significant differences in $\mathrm{PAR_{Gveg}}$ were found between ExL and ExLS at any hour of the day.

3.3. LAI and $\mathrm{LAI_{eff}}$

There were no statistically significant differences among treatments in either LAI or daily integrated $\mathrm{LAI_{eff}}$. The same trend was observed in LAI and $\mathrm{LAI_{eff}}$ among treatments, where values were highest in ExLS and lowest in CT (supp. figure 1). Although there were no statistically significant differences between LAI and mean daily integrated $\mathrm{LAI_{eff}}$ within treatments, the variance of $\mathrm{LAI_{eff}}$ values was between 150% (ExL and ExLS) and 300% (CT) higher than that of LAI.

3.4. Ecosystem carbon fluxes

Daily. Treatment had a statistically significant effect for both the LAI- and $\mathrm{LAI_{eff}}$-derived daily integrated carbon fluxes (figure 5). While GPP $\mathrm{LAI_{eff}}$ was significantly higher in ExL relative to both CT and ExLS, there were no statistically significant differences in $\mathrm{GPP_{LAI}}$ among treatments (figure 5(a)). There

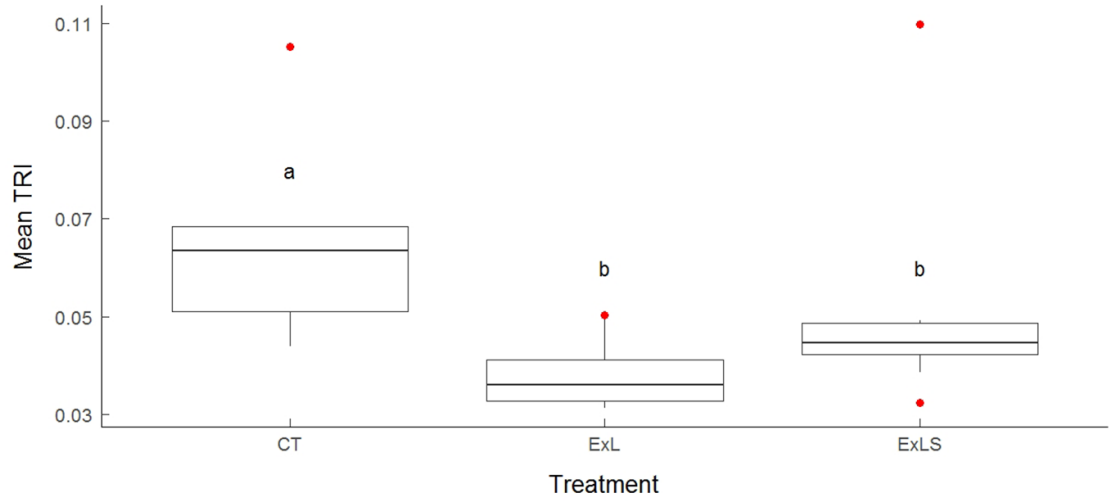

Figure 3. Average terrain ruggedness index (TRI) per treatment. The center black line within each box represents the median TRI value per subplot. Boxes are bound at the 25th and 75th percentiles and whiskers extend to 1.5 * the interquartile range beyond the boxes. Red points indicate outliers that were removed before statistical analyses. Letters indicate significant differences between treatments.

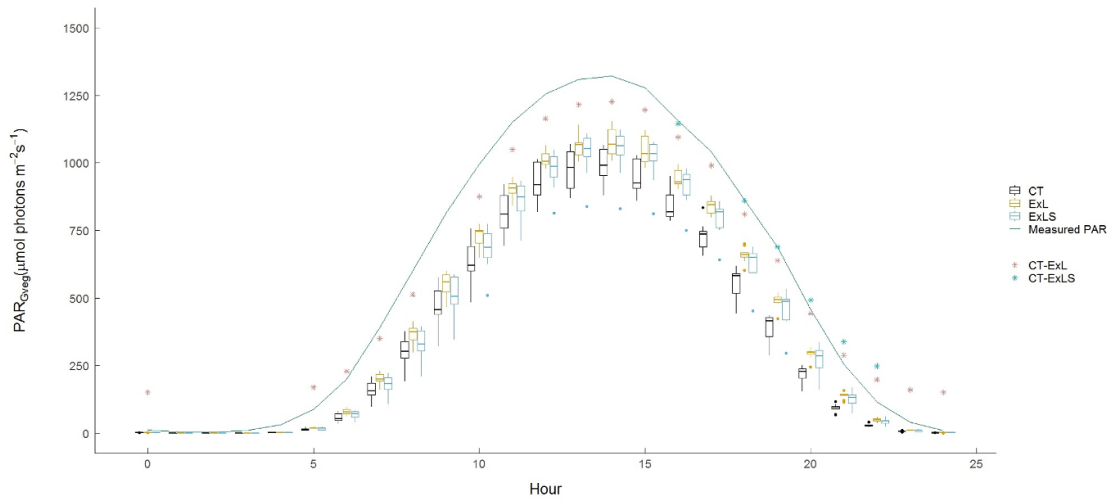

Figure 4. Average hourly PAR received by voxels identified as green vegetation per treatment (PAR_{Gveg}). Boxplots are defined as in figure 3. Significant differences between treatments are indicated by colored asterisks according to the legend.

were statistically significant differences in $NEELAI_{eff}$ among CT (highest; net loss of CO_2 from canopy to atmosphere), ExL (lowest; net gain of CO_2 by canopy from atmosphere) and ExLS (net loss of CO_2 from canopy to atmosphere), while NEE_{LAI} was higher in CT (net loss of CO_2 from canopy to atmosphere) relative to both exclosure treatments (figure 5(b)). There were statistically significant differences between $GPPLAI_{eff}$ and GPP_{LAI} in only ExLS where $GPPLAI_{eff}$ was lower than GPP_{LAI} (figure 5(a)), and between $NEELAI_{eff}$ and NEE_{LAI} where $NEELAI_{eff}$ was both higher and positive (net loss of CO_2 from canopy to atmosphere) relative to NEE_{LAI} which was negative (net gain of CO_2 from atmosphere to canopy) (figure 5(b)). There was little variation in RE fluxes among treatments as the R_0 parameter was near 0 (data not shown).

Hourly. In contrast to daily integrated carbon flux estimates in which only ExLS showed statistically significant differences in LAI_{eff}- compared to LAI-derived values, hourly carbon flux estimates showed strong differences in each of CT, ExL and ExLS (figure 6). In general, GPP LAI_{eff} was lower than GPP_{LAI} during the early morning (~4 am to 7 am) and late evening (~9 pm to 11 pm) hours (figures 6(a), (c) and (e)), and NEE LAI_{eff} values were higher than NEE_{LAI} during those same time periods (figures 6(b), (d) and (f)). There was little variation in RE fluxes among treatments as the R_0 parameter was near 0 (data not shown).

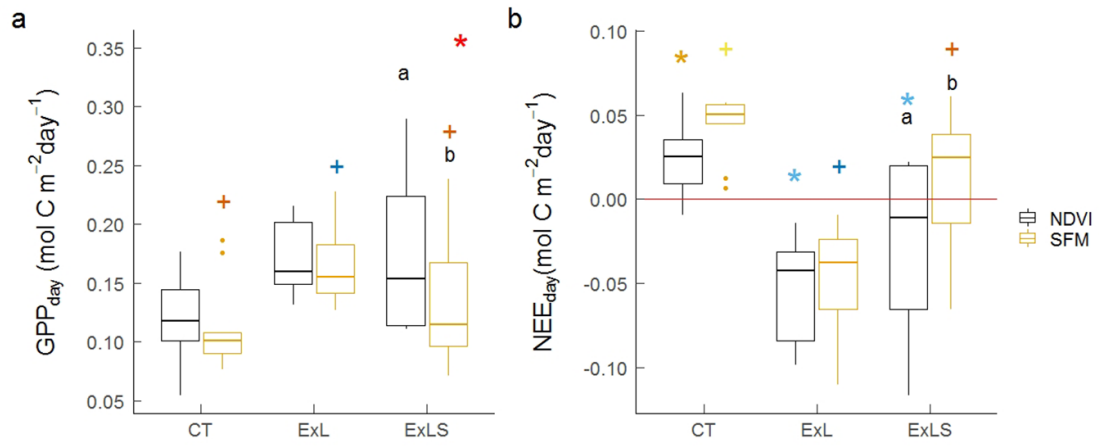

Figure 5. Average daily GPPLAI and $GPPLAI_{eff}$ (a) and NEELAI and $NEELAI_{eff}$ (b) per treatment. Boxplots are defined as in figure 3. Letters indicate significant differences between LAI- and LAI_{eff}-based carbon flux estimates. Colored +s indicate significant differences between treatments for $GPPLAI_{eff}$ and $NEELAI_{eff}$. Colored asterisks indicate significant differences between treatments for GPP_{LAI} and NEE_{LAI}. The red asterisk (a) is to indicate that treatment has a statistically significant effect for GPP_{LAI} but no pairwise comparisons were significant.

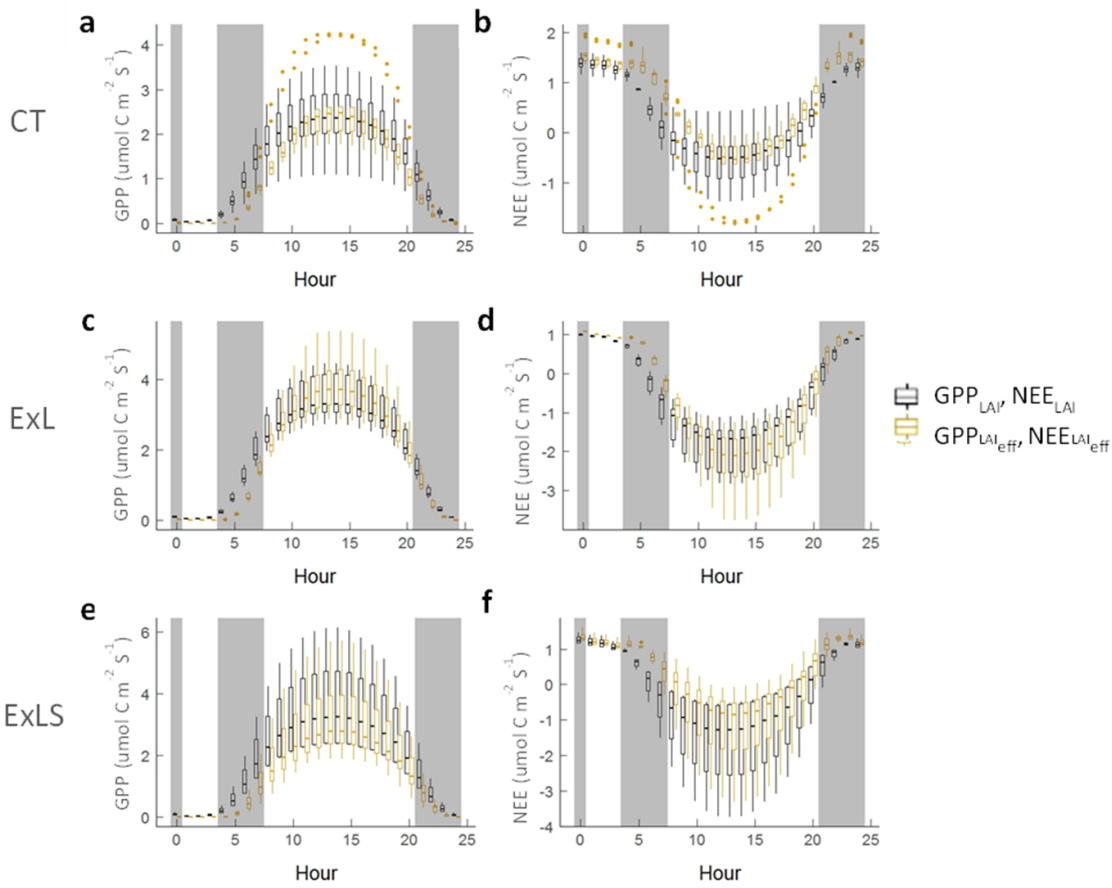

Figure 6. Average hourly GPP_{LAI}, $GPPLAI_{eff}$, NEE_{LAI} and $NEELAI_{eff}$ per treatment. CT averages are shown in (a) and (b). ExL treatment averages are shown in (c) and (d). ExLS treatment averages are shown in (e) and (f). Boxplots are defined as in figure 3. Shaded regions indicate hours where the difference between LAI- and LAI_{eff}-based carbon flux estimates are significantly different.

4. Discussion

Daily rates of canopy CO_2 uptake (i.e. GPP) of dry heath tundra canopies during mid-summer are likely significantly lower compared to those estimated by the majority of tundra studies to date that use LAI and assume uniform light distribution over vegetation canopies throughout the day. By explicitly accounting

for canopy positions of green vegetation and the amount of light that reaches that vegetation over the course of a single day, our results support our hypothesis by demonstrating that the uniquely low sun angles of arctic summers interact with even the low stature of dry heath ecosystems to create long shadows over canopies for large portions of the day. In turn, the reduction of light reaching green vegetation of dry heath canopies limits rates of canopy carbon uptake via photosynthesis, and since shadows do not impose an equivalent limitation in ecosystem respiration, rates of net carbon loss to the atmosphere are likely greater in this tundra type than previously estimated.

Lack of information on 3D canopy structure has been cited as a cause for both over- and underestimations of GPP in a range of ecosystems due to the contribution of shaded foliage to photosynthesis being improperly accounted for (Chen *et al* 2012, Sprintsin *et al* 2012). Although the importance of canopy structure on carbon flux in taller, woody deciduous shrub dominated tundra communities has been previously recognized (Williams *et al* 2014, Magney *et al* 2016), the impact of canopy structure in lower stature and partially vegetated (i.e. LAI $< 1\ m^2\ m^{-2}$) tundra communities, such as dry heath tundra studied herein, has not been considered. Our findings are important as they strongly suggest that even in tundra canopies as simple as dry heath, disregarding the effects of shading introduces inaccuracies into estimates of ecosystem carbon fluxes. In fact, by incorporating canopy structure the current findings can further explain our own previous work in the same dry heath tundra communities and experimental plots (Min *et al* 2021). Previously we used only NDVI-derived estimates of LAI which do not explicitly account for 3D canopy structure and found that despite having lower LAI, the ExL treatment had higher light saturated rates of photosynthesis in mid-summer than the ExLS treatment (Min *et al* 2021). Relative to plots with a higher terrain ruggedness (i.e. CT and ExLS), the smoother ExL treatment not only had lower LAI, but there was little difference in its vegetation composition that would help explain the higher light saturated photosynthetic rates observed by Min *et al* (2021). Instead, our current findings reveal that due to differences in the 3D structure of their canopies, dry heath canopies of the smoother ExL treatment consistently receive higher levels of light due to less shading compared to CT. This suggests that the green vegetation of ExL canopies is well-adapted to high light conditions that support the high rates of light saturated photosynthesis (Laisk *et al* 2005).

Although not the primary purpose of this study, our findings also provide new insight into how herbivores can alter the form and function of tundra communities. Not only do our results show that mammalian herbivores directly alter the 3D canopy structure of dry heath tundra communities, they also suggest that these alterations can result in significant differences in ecosystem carbon fluxes. Moreover, our findings highlight the fact that in these characteristically low productivity ecosystems, even small inaccuracies in estimates of carbon fluxes can affect the prediction of whether tundra communities are net carbon sinks or sources. When variation in 3D canopy structure was *not* explicitly accounted for in estimating NEE, the exclusion of both large and small herbivores (ExLS) was predicted to render dry heath communities net *sinks* for carbon during mid-summer (Min *et al* 2021). In contrast, our current, explicit inclusion of information on 3D canopy structure in estimating NEE reveals that dry heath tundra is predicted to be a net *source* of carbon in the absence of both large and small herbivores (ExLS). In this way, our study strongly suggests that spatial differences and temporal changes in even the structurally simplest arctic tundra canopies should be accounted for to reduce uncertainty in predictions of how tundra vegetation contributes to the biome's overall cycling and storage of carbon. Importantly, although Arctic tundra has been a carbon sink for tens of thousands of years (Miller *et al* 1983, McKane *et al* 1997), its present and future carbon balance remains in question with many studies reporting conflicting findings (Jones *et al* 1998, McGuire *et al* 2012, Fisher *et al* 2014, Euskirchen *et al* 2016, Commane *et al* 2017). Further, the work presented herein adds to a small body of tundra-specific studies that have also demonstrated the effective use of SFM based approaches to better understand the response of arctic tundra's ecological form and function to climate change (e.g. Cunliffe *et al* 2016, Fraser *et al* 2016, Korne *et al* 2020).

Data availability statement

The data that support the findings of this study are openly available at the following URL/DOI: https://portal.edirepository.org/nis/mapbrowse?packageid=knb-lter-arc.20122.1 (Griffin and Boelman 2020). Data will be available from 17 June 2023.

Acknowledgments

The authors thank and acknowledge Toolik Field Station Arctic LTER (NSF Grant # 1637459) for maintaining the long-term herbivore exclosure experiment and CH2MHill Polar Services for their logistical support of this project. This work was supported by funding from the NSF (Grants OPP-1603677 to J R M, OPP-1603760 to L G, OPP-1603654 to R J R, OPP-1603560 to E R, OPP-1603777 to N B and K L G, and DEB-1637459 and DEB-2220863 to K L G, E B R and L G).

ORCID iDs

Elizabeth Min https://orcid.org/0000-0001-7889-6693
Shahid Naeem https://orcid.org/0000-0002-6569-2648
Laura Gough https://orcid.org/0000-0002-9312-7910
Jennie R McLaren https://orcid.org/0000-0003-2004-4783
Rebecca J Rowe https://orcid.org/0000-0002-0492-568X
Edward Rastetter https://orcid.org/0000-0002-8620-5431
Natalie Boelman https://orcid.org/0000-0003-3716-2372
Kevin L Griffin https://orcid.org/0000-0003-4124-3757

References

Alonzo M, Dial R J, Schulz B K, Andersen H E, Lewis-Clark E, Cook B D and Morton D C 2020 Mapping tall shrub biomass in Alaska at landscape scale using structure-from-motion photogrammetry and Lidar *Remote Sens. Environ.* **245** 111841

Bates D, Mächler M, Bolker B M and Walker S C 2015 Fitting linear mixed-effects models using lme4 *J. Stat. Softw.* **67** 1–48

Boelman N T, Gough L, McLaren J R and Greaves H 2011 Does NDVI reflect variation in the structural attributes associated with increasing shrub dominance in arctic tundra? *Environ. Res. Lett.* **6** 035501

Bréda N J J 2003 Ground-based measurements of leaf area index: a review of methods, instruments and current controversies *J. Exp. Bot.* **54** 2403–17

Brunner A 1998 A light model for spatially explicit forest stand models *For. Ecol. Manage.* **107** 19–46

Buchhorn M, Raynolds M K and Walker D A 2016 Influence of BRDF on NDVI and biomass estimations of Alaska Arctic tundra *Environ. Res. Lett.* **11** 125002

Chen J M, Mo G, Pisek J, Liu J, Deng F, Ishizawa M and Chan D 2012 Effects of foliage clumping on the estimation of global terrestrial gross primary productivity *Glob. Biogeochem. Cycles* **26** 1–18

Commane R, Lindaas J, Benmergui J, Luus K A, Chang R Y W, Daube B C and Wofsy S C 2017 Carbon dioxide sources from Alaska driven by increasing early winter respiration from Arctic tundra *Proc. of the National Academy of Sciences* vol 114 pp 5361–6

Cunliffe A M, Assmann J J, Daskalova G N, Kerby J T and Myers-Smith I H 2020 Aboveground biomass corresponds strongly with drone-derived canopy height but weakly with greenness (NDVI) in a shrub tundra landscape *Environ. Res. Lett.* **15** 125004

Cunliffe A M, Brazier R E and Anderson K 2016 Ultra-fine grain landscape-scale quantification of dryland vegetation structure with drone-acquired structure-from-motion photogrammetry *Remote Sens. Environ.* **183** 129–43

Environmental Data Center Team 2017 Meteorological monitoring program at Toolik, Alaska *Toolik Field Station* (Fairbanks, AK: Institute of Arctic Biology University Alaska Fairbanks) (available at: http://toolik.alaska.edu/edc/weather/data_query.php)

Euskirchen E S, Bret-Harte M S, Shaver G R, Edgar C W and Romanovsky V E 2016 Long-term release of carbon dioxide from Arctic tundra ecosystems in Alaska *Ecosystems* **20** 960–74

Fisher J B *et al* 2014 Carbon cycle uncertainty in the Alaskan Arctic *Biogeosciences* **11** 4271–88

Forlani G, Dall'Asta E, Diotri F, Di Cella U M, Roncella R and Santise M 2018 Quality assessment of DSMs produced from UAV flights georeferenced with on-board RTK positioning *Remote Sens.* **10** 311

Fraser R H, Olthof I, Lantz T C and Schmitt C 2016 UAV photogrammetry for mapping vegetation in the low-Arctic *Arct. Sci.* **2** 79–102

Friedli M, Kirchgessner N, Grieder C, Liebisch F, Mannale M and Walter A 2016 Terrestrial 3D laser scanning to track the increase in canopy height of both monocot and dicot crop species under field conditions *Plant Methods* **12** 1–15

Goh T Y, Basah S N, Yazid H, Safar M J A and Saad F S A 2018 Performance analysis of image thresholding: Otsu technique *Measurement* **114** 298–307

Gough L, Ramsey E A and Johnson D R 2007 Plant-herbivore interactions in Alaskan arctic tundra change with soil nutrient availability *Oikos* **116** 407–18

Greaves H E, Vierling L A, Eitel J U, Boelman N T, Magney T S, Prager C M and Griffin K L 2015 Estimating aboveground biomass and leaf area of low-stature Arctic shrubs with terrestrial LiDAR *Remote Sens. Environ.* **164** 26–35

Griffin K and Boelman N 2020 Carbon dioxide flux measurements from Arctic LTER Heath Tundra herbivore exclosures, Toolik Field Station, Alaska 2013 ver 1. (Environmental Data Initiative) (https://doi.org/10.6073/pasta/3319313d52f5da852316567b2a5c0cad) (Accessed 25 April 2023)

Hijmans R J *et al* 2015 Raster: geographic data analysis and modeling *R Package 734* p 473

Iglhaut J, Cabo C, Puliti S, Piermattei L, O'Connor J and Rosette J 2019 Structure from motion photogrammetry in forestry: a review *Curr. For. Rep.* **5** 155–68

Johnson L C, Shaver G R, Cades D H, Rastetter E, Nadelhoffer K, Giblin A, Laundre J and Stanley A 2000 Plant carbon-nutrient interactions control CO_2 exchange in Alaskan wet sedge tundra ecosystems *Ecology* **81** 453–69

Jones M H, Fahnestock J T, Walker D A, Walker M D and Welker J M 1998 Carbon dioxide fluxes in moist and dry arctic tundra during the snow-free season: responses to increases in summer temperature and winter snow accumulation *Arct. Alp. Res.* **30** 373–80

Kataoka T, Kaneko T, Okamoto H and Hata S 2003 Crop growth estimation system using machine vison *Proc. 2003 IEEE/ASME Int. Conf. on Advanced Intelligent Mechatronics (AIM 2003)* vol 2 (IEEE) pp b1079–83

Koppal S J 2014 Lambertian reflectance *Computer Vision* ed K Ikeuchi (Boston, MA: Springer) (https://doi.org/10.1007/978-0-387-31439-6_534)

Korne N, Flemming S A, Smith P A and Nol E 2020 Applying structure-from-motion habitat reconstruction and GIS terrain analysis to test hypotheses about nest-site selection by shorebirds *J. Field Ornithol.* **91** 421–32

Kramer K, Leinonen I, Bartelink H H, Berbigier P, Borghetti M, Bernhofer C and Vesala T 2002 Evaluation of six process-based forest growth models using eddy-covariance measurements of CO_2 and H_2O fluxes at six forest sites in Europe *Glob. Change Biol.* **8** 213–30

Kuznetsova A, Brockhoff P B and Christensen R H B 2017 lmerTest package: tests in linear mixed effects models *J. Stat. Softw.* **82** 1–26

Laisk A, Eichelmann H, Oja V, Rasulov B, Padu E, Bichele I, Pettai H and Kull O 2005 Adjustment of leaf photosynthesis to shade in a natural canopy: rate parameters *Plant Cell Environ.* **28** 375–88

Lenth R V 2016 Least-squares means: the R package lsmeans *J. Stat. Softw.* **69** 1–33

Magney T S et al 2016 LiDAR canopy radiation model reveals patterns of photosynthetic partitioning in an Arctic shrub *Agric. For. Meteorol.* **221** 78–93

Mao W, Wang Y and Wang Y 2003 Real-time detection of between-row weeds using machine vision *ASAE Annual Meeting American Society of Agricultural and Biological Engineers*

Massa G, Graham T, Haire T, Flemming C II, Newsham G and Wheeler R 2015 Light-emitting diode light transmission through leaf tissue of seven different crops *HortScience Horts* **50** 501–6

Mathews A J and Jensen J L R 2013 Visualizing and quantifying vineyard canopy LAI using an unmanned aerial vehicle (UAV) collected high density structure from motion point cloud *Remote Sens.* **5** 2164–83

McGuire A D et al 2012 An assessment of the carbon balance of Arctic tundra: comparisons among observations, process models, and atmospheric inversions *Biogeosciences* **9** 3185–204

McKane R B, Rastetter E B, Shaver G R, Knute J, Giblin A E, Laundre J A and Chapin F S 1997 Climatic effects on tundra carbon storage inferred from experimental data and a model *Ecology* **78** 1170–87

Mesas-Carrascosa F J, de Castro A I, Torres-Sánchez J, Triviño-Tarradas P, Jiménez-Brenes F M, García-Ferrer A and López-Granados F 2020 Classification of 3D point clouds using color vegetation indices for precision viticulture and digitizing applications *Remote Sens.* **12** 317

Meyer G E, Hindman T W and Laksmi K 1999 Machine vision detection parameters for plant species identification *Precis. Agric. Biol. Qual.* **3543** 327–35

Miller P C, Kendall R and Oechel W C 1983 Simulating carbon accumulation in northern ecosystems *Simulation* **40** 119–31

Min E, Wilcots M E, Naeem S, Gough L, McLaren J R, Rowe R J, Rastetter E B, Boelman N T and Griffin K L 2021 Herbivore absence can shift dry heath tundra from carbon source to sink during peak growing season *Environ. Res. Lett.* **16** 024027

Monsi M, Saeki T and Schortemeyer M 2005 On the factor light in plant communities and its importance for matter production *Ann. Bot.* **95** 549–67

Morgan-Wall T 2020 R package rayshader: create maps and visualize data in 2D and 3D (available at: https://github.com/tylermorganwall/rayshader)

Neto J C 2004 *A Combined Statistical-Soft Computing Approach for Classification and Mapping Weed Species in Minimum-Tillage Systems* (Lincoln, NE: The University of Nebraska-Lincoln)

Omasa K, Hosoi F and Konishi A 2007 3D Lidar imaging for detecting and understanding plant responses and canopy structure *J. Exp. Bot.* **58** 881–98

Rastetter E B et al 2010 Processing arctic eddy-flux data using a simple carbon-exchange model embedded in the ensemble Kalman filter *Ecol. Appl.* **20** 1285–301

Roussel J R, Auty D, Coops N C, Tompalski P, Goodbody T R H, Meador A S, Bourdon J F, de Boissieu F and Achim A 2020 lidR: an R package for analysis of airborne laser scanning (ALS) data *Remote Sens. Environ.* **251** 112061

Shafian S, Rajan N, Schnell R, Bagavathiannan M, Valasek J, Shi Y and Olsenholler J 2018 Unmanned aerial systems-based remote sensing for monitoring sorghum growth and development *PLoS One* **13** e0196605

Shaver G R, Street L E, Rastetter E B, Van Wijk M T and Williams M 2007 Functional convergence in regulation of net CO_2 flux in heterogeneous tundra landscapes in Alaska and Sweden *J. Ecol.* **95** 802–17

Shaver G and Chapin F S 1991 Production: biomass relationships and element cycling in contrasting Arctic vegetation types *Ecol. Monogr.* **61** 1–31

Sprintsin M, Chen J M, Desai A and Gough C M 2012 Evaluation of leaf-to-canopy upscaling methodologies against carbon flux data in North America *J. Geophys. Res.* **117** 1–17

Stow D A et al 2004 Remote sensing of vegetation and land-cover change in Arctic Tundra ecosystems *Remote Sens. Environ.* **89** 281–308

Stow D, Hope A, Boynton W, Phinn S, Walker D and Auerbach N 1998 Satellite-derived vegetation index and cover type maps for estimating carbon dioxide flux for arctic tundra regions *Geomorphology* **21** 313–27

Stoy P, Williams M, Evans J, Prieto-Blanco A, Disney M, Hill T, Ward H, Wade T and Street L 2013 Upscaling tundra CO_2 exchange from chamber to eddy covariance tower *Arct. Antarct. Alp. Res.* **45** 275–84

Street L E, Shaver G R, Williams M and Van Wijk M T 2007 What is the relationship between changes in canopy leaf area and changes in photosynthetic CO_2 flux in arctic ecosystems? *J. Ecol.* **95** 139–50

Team R C 2013 R development core team *R: A Language and Environment for Statistical Computing* vol 55 pp 275–86

US Department of Commerce, NOAA and Laboratory G M 2005 ESRL global monitoring laboratory—global radiation and aerosols (available at: www.esrl.noaa.gov/gmd/grad/solcalc/)

Verhoef W 1984 Light scattering by leaf layers with application to canopy reflectance modeling: the SAIL model *Remote Sens. Environ.* **16** 125–41

Virkkala A M, Virtanen T, Lehtonen A, Rinne J and Luoto M 2018 The current state of CO_2 flux chamber studies in the Arctic tundra: a review *Prog. Phys. Geogr.* **42** 162–84

Wall S D, Farr T G, Muller J P, Lewis P and Leberl F W 1991 Measurement of surface microtopography *Photogramm. Eng. Remote Sens.* **57** 1075–8 (available at: www.asprs.org/wp-content/uploads/pers/1991journal/aug/1991_aug_1075-1078.pdf)

Weiss M, Baret F, Smith G J, Jonckheere I and Coppin P 2004 Review of methods for *in situ* leaf area index (LAI) determination part II. Estimation of LAI, errors and sampling *Agric. For. Meteorol.* **121** 37–53

Westoby M J, Brasington J, Glasser N F, Hambrey M J and Reynolds J M 2012 "Structure-from-motion" photogrammetry: a low-cost, effective tool for geoscience applications *Geomorphology* **179** 300–14

Williams M, Rastetter E B, Van der Pol L and Shaver G R 2014 Arctic canopy photosynthetic efficiency enhanced under diffuse light, linked to a reduction in the fraction of the canopy in deep shade *New Phytol.* **202** 1267–76

Woebbecke D M, Meyer G E, Von Bargen K and Mortensen D A 1993 Plant species identification, size, and enumeration using machine vision techniques on near-binary images David *Opt. Agric. For.* **1836** 208–19

Woebbecke D M, Meyer G E, Von Bargen K and Mortensen D A 1995 Color indices for weed identification under various soil, residue, and lighting conditions *Trans. ASAE* **38** 259–69

Zellweger F, De Frenne P, Lenoir J, Rocchini D and Coomes D 2019 Advances in microclimate ecology arising from remote sensing *Trends Ecol. Evol.* **34** 327–41

Zulueta R C, Oechel W C, Loescher H W, Lawrence W T and Paw K T 2011 Aircraft-derived regional scale CO_2 fluxes from vegetated drained thaw-lake basins and interstitial tundra on the Arctic Coastal Plain of Alaska *Glob. Change Biol.* **17** 2781–802